Smart Structures and Systems, *Vol. 28, No. 3 (2021) 333-341*
https://doi.org/10.12989/sss.2021.28.3.333

Development of wireless SHM sensor node for in-flight real-time monitoring using embedded CNT fiber sensors

Jinwoo Park [1a], Yeol-Hun Sung [1b], Seung Yoon On [2a], O-Hyun Kwon [3a], Hyochoong Bang [1c], Seong Su Kim [2c], Jae-Hung Han [1c] and Jung-Ryul Lee*[1]

[1] *Department of Aerospace Engineering, Korea Advanced Institute of Science and Technology, 291 Daehak-ro, Yuseong-gu, Daejeon 34141, Republic of Korea*
[2] *Department of Mechanical Engineering, Korea Advanced Institute of Science and Technology, 291 Daehak-ro, Yuseong-gu, Daejeon 34141, Republic of Korea*
[3] *School of Aerospace and Mechanical Engineering, Korea Aerospace University, 76 Hanggongdaehak-ro, Deogyang-gu, Goyang-si, Gyeonggi-do 10540, Republic of Korea*

(*Received July 2, 2020, Revised January 21, 2021, Accepted March 22, 2021*)

Abstract. Structural health monitoring (SHM) is essential for composite unmanned aerial vehicles (UAVs). Additionally, because UAVs are extremely sensitive to weight and volume, the minimal addition of weight and volume by the SHM system is crucial. Therefore, we proposed a compact and lightweight wireless SHM sensor node and an embedded carbon nanotube (CNT) fiber sensor for in-flight SHM of UAVs. The wireless SHM sensor node was composed of an analog sensing circuit, wireless microcontroller unit, and analog low pass filter. The small diameter CNT fiber sensor was developed to be easily embedded inside composite structures and to enhance their structural properties while performing as an SHM sensor. Glass composite skin with embedded CNT fiber sensors composed of ultra-high-molecular-weight polyethylene, polyurethane, CNT, and carbon black were installed in the aircraft. For comparison, a strain gauge attached at the center of a long CNT fiber sensor was also used during in-flight measurement. In-flight strain measurements from both the CNT fiber sensor and the strain gauge were continuously transmitted to the ground station and were compared with the flight data. Furthermore, an impact tester was installed inside the wing to simulate impact during flight, and in-flight impact measurements by the CNT fiber sensor were demonstrated.

Keywords: structural health monitoring; wireless sensor node; carbon nanotube fiber sensor; in-flight real-time monitoring

1. Introduction

Composite materials are frequently used in modern aircraft structures, particularly in small aircrafts, such as unmanned aerial vehicles (UAVs) and drones. The advantages of a composite aircraft structure are its low weight, high strength, and high stiffness (Staszewki *et al*. 2009 and Herszberg *et al*. 2007). Additionally, owing to the development of manufacturing technology and the process of creating composite structures, complex aerodynamic shapes that were impossible to achieve with conventional alloy steel structures are now possible with composite materials. The properties of these materials have led to a significant increase in the usage of glass fiber-reinforced polymer (GFRP) composite structures in UAVs and drones. However, composite structures have a high risk of structural failure when exposed to sudden impacts or loading, which can cause defects, such as cracks or delamination, and catastrophic accidents (Botelho *et al*. 2006 and Hassan *et al*. 2017). Therefore, structural health monitoring (SHM) of these composite structures is needed to monitor the integrity of the aircraft and prevent structural failure.

For SHM during the flight of an aircraft, various sensors are used to obtain the desired measurements. The most common and widely used sensor for strain measurement is the strain gauge. Strain gauges are cost effective and come in various types and sizes for different types of measurements and situations. But the installation of strain gauges is laborious and has a high dependency on the process of attachment which may result in inconsistence in the sensor's performance. Fiber Bragg grating (FBG) sensors have been used as an alternative for strain gauges for SHM. FBG sensors measure strain by demodulating the wavelength shift. FBG sensors are nonconductive and are immune to electromagnetic interference, which can be highly effective for reducing noise level or interference in sensor measurements. However, owing to the fact that they measure wavelengths, the measurement setup is complex, expensive, and inappropriate for on-board measurement in aircrafts during flight (Molent and Aktepe 2000).

Carbon nanotube (CNT) fiber sensors have been

*Corresponding author, Professor,
E-mail: leejrr@kaist.ac.kr
[a] Ph.D. Student
[b] Ph.D., Currently at Aeronautics Technology Research Division, Korea Aerospace Research Institute
[c] Professor

ISSN: 1738-1584 (Print), 1738-1991 (Online)

investigated owing to their unique mechanical and electrical properties. When embedded in composite materials, CNT fiber sensors can increase the tensile strength owing to their excellent mechanical properties (Zhu *et al*. 2017). Additionally, CNT fiber sensors have a smaller diameter in comparison with FBG sensors, which is essential when embedding the sensor within the composite layers (Takeda *et al*. 2005). Furthermore, in comparison with attachment sensors, embedded sensors can reduce the overall weight and volume of the system and ensure consistent operating certainty.

SHM sensor nodes measure and digitize the analog signal from the sensors and store or transfer the data to the database server. Previous research has tested SHM during flight by attaching sensors to the aircraft. Tang *et al*. (2010) developed a monitoring system for the landing gear of the aircraft by attaching strain gauges. Strain measurements during take-off and landing were acquired. Kim *et al*. (2015) implemented a health and usage monitoring system (HUMS) using FBG sensors and evaluated in-flight strain monitoring of an aircraft. Kwon *et al*. (2019) installed FBG sensors in the main wing of an aircraft to obtain wing loading measurements. Small aircrafts, such as UAVs, have also been outfitted with SHM systems to monitor in-flight measurements. Kressel *et al*. (2012) investigated an SHM system capable of real-time data processing and load tracking. FBG sensors were installed in the UAV tail boom and FBG measurements during flight and landing were acquired. All the above studies have used wired SHM systems with internal storage devices storing the SHM data during flight, and require the manual transfer of data after the flight. In contrast, Alvarez-Montoya *et al*. (2019) conducted wireless SHM using 20 FBG sensors installed inside the main wing of a UAV. A wireless local area network (WLAN) with a 15 dBi antenna for the ground station and a 5 dBi antenna for the UAV was used for the wireless protocol. However, usage of the FBG sensors with a circulator, beam splitter, and optical interrogator increased the overall payload weight and volume. Additionally, usage of the WLAN wireless protocol limited the wireless transmission range and power usage of the aircraft, which can be restricted for adapting to UAVs with a larger operation radius.

In this study, a compact and lightweight wireless SHM sensor node was developed for UAVs. The wireless SHM sensor node could interrogate CNT fiber sensors with high resistances embedded inside the aircraft using a long-range wireless protocol capable of transmissions up to a few kilometers. The wireless SHM sensor node used 868 MHz frequency band with Texas Instrument's long range wireless protocol (Sub 1 GHz proprietary RF protocol). The integrity of wirelessly transmitted data was ensured by pretests on ground before flight test. Samples were acquired in real time during the flight with a continuous 100 Hz sampling frequency for strain measurements and a 100 kHz sampling frequency for impact measurements. Strain measurements were obtained from harsh pitch maneuvers of the aircraft and impact signals which was excited by an on-board impactor were successfully acquired during the flight.

2. Wireless SHM sensor node

2.1 Usability of wireless SHM sensor node

UAVs and drones have more restricted and smaller operational radii compared to conventional aircrafts. This can be due to a lack of fuel, battery size, restricted communication range for controlling the vehicle, or particular objectives, such as surveillance or small cargo transportation. This smaller operational radius can be an advantage in the implementation of a wireless SHM system, which can enhance the safety of the aircraft itself and the environment within the operational radius. However, conventional SHM systems consist of a large data acquisition system and a data storage system (Zhou *et al*. 2010). Not only do these kinds of SHM systems decrease the payload capacity of the operational range of the UAVs, but they also fail to ensure the structural integrity of the UAVs in real time. Therefore, while maintaining a compact

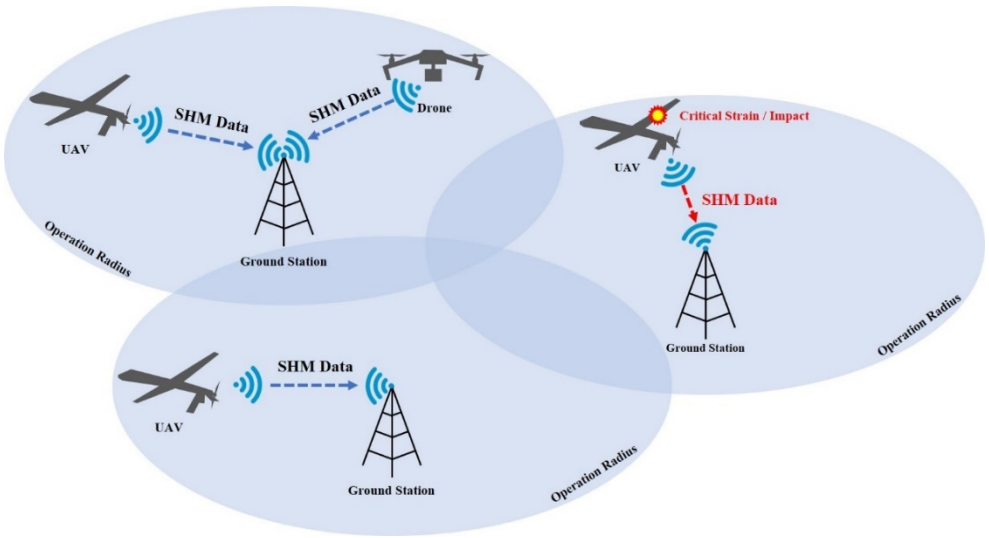

Fig. 1 Schematic of wireless SHM sensor node being used for UAVs and drones

and lightweight system without harming the performance of the UAV, the wireless SHM sensor node must be capable of consistent real-time monitoring of the structure of the aircraft. Moreover, for a compact and lightweight SHM system, the SHM sensor node and the SHM sensors are important factors for implementation on small UAVs. In addition, conventional SHM sensors were attached to the structures, meaning that multiple sensors with connecting wires could increase the overall SHM system weight and volume which could decrease the capability of the UAVs. Attachment sensors can also be highly dependent on the attachment process, and the future maintenance process for checking the integrity of the attachment increases the overall maintenance cost and time. Therefore, in this study, composite skin embedded with CNT fiber sensors were used to minimize the additional weight and volume of the SHM system and increase the mechanical properties of the composite structures.

2.2 Wireless SHM sensor node measurement and transmission

The wireless SHM sensor node developed for this study consisted of an analog sensing circuit, analog low pass filter, and wireless MCU, as shown in Fig. 2. The variable quarter-bridge circuit inside the analog sensing circuit consisted of three identical fixed resistors as reference resistance. Since the MCU's analog to digital converter (ADC) was only capable of measuring positive voltage, a potentiometer (variable resistance) was used to match the small difference between the reference resistance and the resistance of the CNT fiber sensor. The need for a potentiometer was inevitable because even the most accurate of fixed resistors on the market had a 0.1% error, resulting in an output voltage outside of the measurement range of the MCU. Therefore, the resistance value of the potentiometer was 1% of the value of the reference resistance and a serial connection of the potentiometer with a smaller value was used to balance the bridge and allow an offset voltage of the output for measurement with the MCU ADC.

The embedded CNT fiber sensor exhibited a significantly high resistance in comparison with the conventional resistance sensors. The analog sensing circuit for measuring the CNT fiber sensor consisted of Texas Instrument's INA333 instrumentation amplifier. The large common-mode rejection ratio (CMRR) and the very high input impedance from two buffer amplifiers of zero-drift OPA333 operational amplifier inside the instrumentation amplifier enabled precise measurements of the CNT fiber sensor with high resistance. Additionally, the use of an electromagnetic interference (EMI)-hardened instrumentation amplifier was crucial due to the high wireless transmission power and low current of the input signal from the CNT fiber sensor's high resistance. Without EMI resistance, the wireless transmission itself interferes with the electromagnetic field around the sensor, which according to Faraday's law, interferes with the current going through the CNT fiber sensor and influences the output voltage. For the low resistance sensor, this factor is negligible since the current passing through the sensor is large compared to the change of current induced from the electromagnetic change from the wireless transmission. For instance, with a 3.3 V excitation voltage, a 100 Ω sensor will have 33 mA of current passing though the sensor. In the case of the CNT fiber sensor, the resistance value is in the range of hundreds of kiloohms. Therefore, if the CNT fiber sensor has 100 kΩ of resistance with a 3.3 V excitation voltage, the current passing through the sensor will be 33 nA. Furthermore, because the input signal for the instrumentation was extremely sensitive to the noise level, an ultra-low-noise low dropout linear regulator power supply was selected to supply constant low noise 3.3 V for the whole SHM sensor node by a single cell of a lithium-ion battery (3.7 V). The average power consumption of single wireless SHM sensor node was 74 mW when using 3.7 V single cell lithium ion battery. A 3000 mAh 18650 lithium ion battery was capable of operating the wireless SHM sensor node up to 150 hours, which was more than enough for multiple flight tests. The average power consumption of single wireless SHM sensor node was 74 mW when using 3.7 V single cell lithium ion battery. A 3000 mAh 18650 lithium ion battery was capable of operating the wireless SHM sensor node up to 150 hours, which was more than enough for multiple flight tests. Therefore, careful selection and design of the printed circuit board (PCB) layout of the analog circuit for minimizing the interference and noise level was undertaken to measure the CNT fiber sensor's input signal. The input signal (differential signal from the quarter-bridge circuit) was amplified by the maximum gain factor 1000 to match the

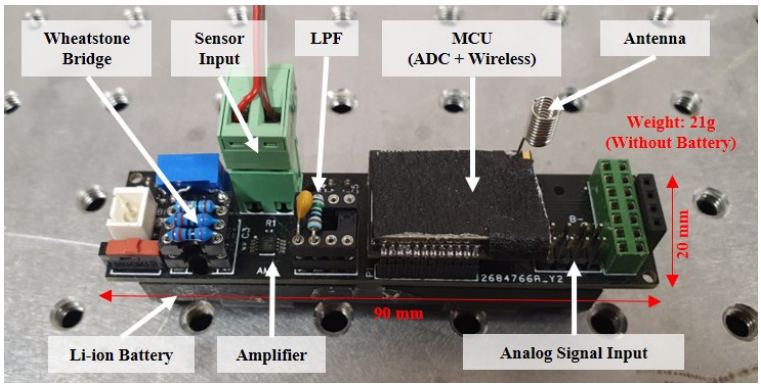

Fig. 2 Wireless SHM sensor node

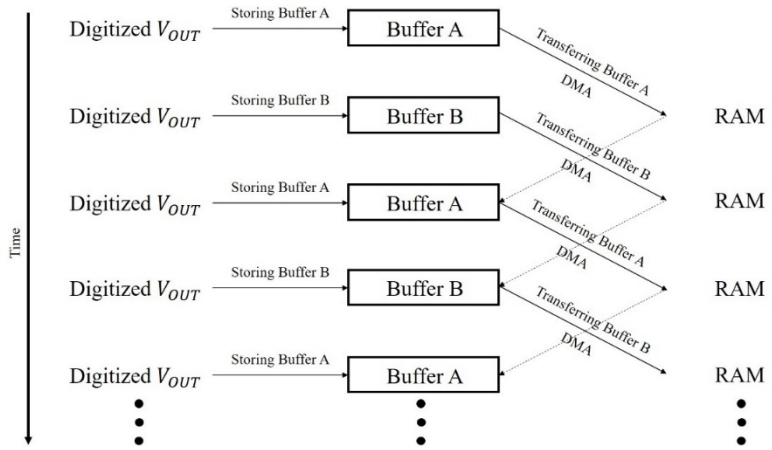

Fig. 3 Schematic of double buffering method using DMA

input voltage range of the MCU and was calibrated to measure up to 1000 με for CNT fiber sensor measurements with a resolution of 0.5 με using Eq. (1).

$$Strain\ (\varepsilon) = \frac{-4\left(\frac{V_{OUT(strained)}-V_{OUT(unstrained)}}{V_{EX}}\right)}{GF\left\{1+2\left(\frac{V_{OUT(strained)}-V_{OUT(unstrained)}}{V_{EX}}\right)\right\}} \quad (1)$$

To enable continuous measurement of the analog signal, a double buffering method was used and direct memory access (DMA) transfer of the measured data was performed. Fig. 3 shows the double buffering method with DMA, where 50 data points were assigned to a unit buffer that alternated from storing the 50 measured data points to transmitting wirelessly to the receiver in the ground station. Therefore, when the first unit buffer finished measuring and storing 50 data points, the second unit buffer started to measure and store data points, and the first unit buffer transferred its data to the wireless transmitter. This transmission was completed before the second unit buffer completed its measurement.

The use of these two methods was inevitable since commercial MCUs have limited random access memory (RAM) sizes and low MCU processing power. Due to conventional usage and low cost of the MCU, the RAM size of the MCU is restricted to a few hundred kilobytes. The small size of the RAM restricted the total number of measurement points to a few thousand. In order to increase the length of the measurement, addition of more RAM was possible. However, this method increases the size and power consumption of the sensor node which was not optimal for this application. Also, low MCU processing power decreased the maximum sampling frequency when the MCU was involved in data transfer from ADC to RAM. The maximum clock speed of the MCU used in the wireless SHM sensor node was only 48 MHz. Without DMA, the maximum sampling frequency for 2000 points were 2 kHz. Exceeding 2 kHz sampling frequency resulted discontinuity between every unit buffer (50 data points). On the other hand, DMA enables direct transfer from ADC to RAM which does not involve the MCU processing, which enabled maximum sampling frequency for 2000 points up to 100 kHz. Therefore, using the double buffering method and DMA, the measured data points of each unit buffer were transferred via wireless transmission without any bottleneck and an excessive number of data points did not accumulate in the MCU RAM.

The measured data was then transferred by the sub 1 GHz wireless transmission inside the MCU in a half word packet and the receiver decoded the data into the strain value at the ground station. The sub 1 GHz wireless protocol used in this MCU had a communication range of several kilometers. The range was highly dependent on the antenna size and environmental electromagnetic interference. For this in-flight measurement, a small helix coil antenna with a diameter of 5 mm and a height of 6 mm was used to reduce the volume capacity. The maximum communication range was found to be 2 km on the ground with a clear line of sight using this small helix coil antenna. The integrity of the transmitted data was ensured by verifying that the number of sent data samples from the transmitter matched the number of received data samples from the receiver for both 100 Hz and 100 kHz sampling frequency. Each wireless SHM sensor node was connected to single CNT fiber sensor. In this flight test, total of two wireless SHM sensor node was used for strain and impact measurements. 868 MHz and 870 MHz were used as radio frequency and the 2 MHz frequency difference showed no interference with each other.

For strain measurements, the sampling frequency was 100 Hz and passive analog low pass filter with 5 Hz cutoff frequency was applied. Fig. 4(a) shows the algorithm for the 100 Hz sampling frequency for the wireless SHM sensor node. The process of each unit buffer measuring and storing 50 data points and transmitting wirelessly was completed in 0.5 s, meeting the requirements for the continuous 100 Hz measurements without excessive data accumulating in the MCU memory during the measurements.

For impact measurement, another wireless SHM sensor node was prepared and the sampling frequency was 100 kHz and analog low pass filter with 10 kHz cutoff frequency was applied. Fig. 4(b) shows the algorithm for

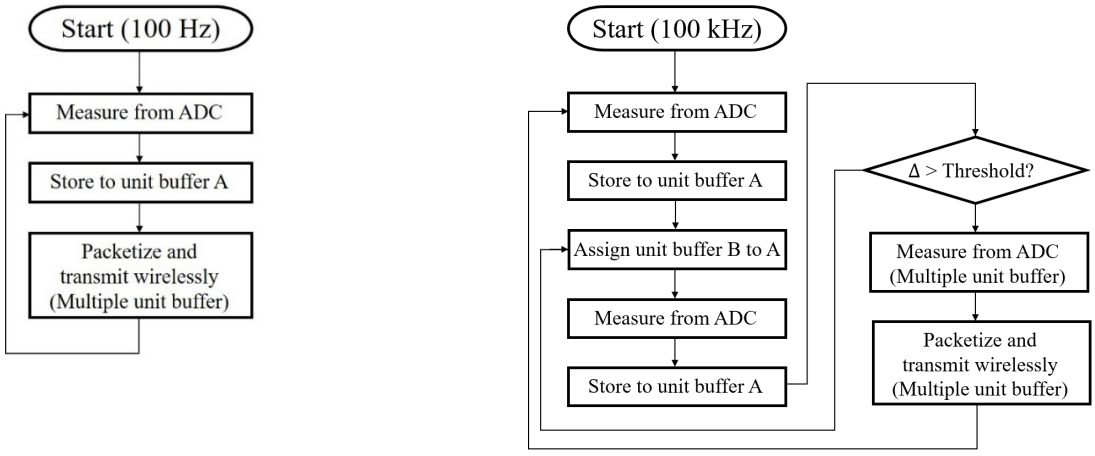

(a) 100 Hz sampling rate (b) 100 kHz sampling rate

Fig. 4 Algorithm of wireless SHM sensor node measurements

the 100 kHz sampling frequency for the wireless SHM sensor node. Since the maximum repetition rate of the wireless transmission was 0.1 s, a 100 kHz sampling frequency was too high to transfer all of the measured data. Therefore, a self-triggering method was used to measure and transmit 2000 data in 20 ms. For the self-triggering method, two unit buffers were constantly measuring the input signal to detect a sudden peak. The peak amplitude of the input signal was compared with a predefined threshold to determine whether to recognize the difference as an impact and capture the subsequent data points. Since the slope or the amplitude of the threshold is adjustable depending on the input signal, a trial and error method was used to find the optimal value for detecting the impact signal before the flight test.

3. CNT fiber sensor embedded aircraft

3.1 GFRP skin with embedded CNT fiber sensor

The proposed CNT fiber sensor consisted of two layers of a polyurethane (PU), a multi-walled CNT coating layer, and core fiber. Fig. 5(a) shows the composition of the sensor: core fiber of ultra-high-molecular-weight polyethylene (UHMWPE), which was coated with the first PU layer, a CNT layer containing carbon black (CB), and the second PU layer. The first PU coating layer was added to increase the friction between the UHMWPE core fiber and the CNT/CB coating layer. Without the first PU coating layer, the UHMWPE core fiber and the CNT/CB coating layer tended to slip, resulting in no change in the resistance during the tension and compression of the CNT fiber sensor.

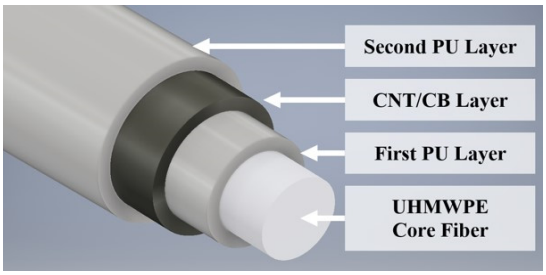

(a) Schematic of CNT fiber sensor

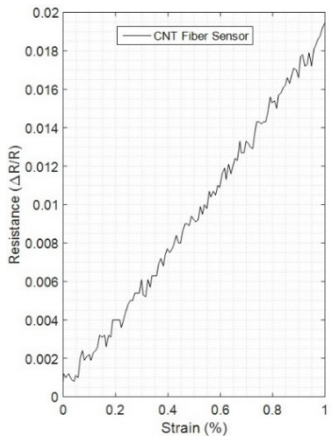

(b) Gauge factor of CNT fiber sensor

Fig. 5 CNT fiber sensor

This was because of the fact that during deformation of the CNT fiber sensor, only the core fiber was deformed, and not the CNT coating layer, which altered the resistance value. An increase in the CB concentration decreased the

Table 1 CNT fiber sensor characteristics

Length (mm)	Thickness (μm)	Resistance (Ω/mm)	Tensile strength (MPa)	Tensile modulus (GPa)	Gauge factor
300 (Strain Measurement) 200 (Impact Measurement)	80	700	501	7.6	2.0

(a) Schematic of GFRP skin (b) GFRP skin

Fig. 6 GFRP skin with embedded CNT fiber sensor

resistance value and gauge factor of the sensor. Because the increase in the resistance of the CNT fiber sensor increased the noise level and a high gauge factor was needed for sensitive strain measurement, multiple CB concentrations were tested and the optimal CB concentration was found to be at 0.25 wt% (On *et al*. 2019). Table 1 presents the characteristics of the CNT fiber sensor used in this application with a thickness of 80 μm, resistance of 700 Ω/mm, tensile strength of 501 MPa, tensile modulus of 7.6 GPa, and gauge factor of 2.0.

The CNT fiber sensor was embedded inside a GFRP with four plies of glass unidirectional prepregs in a stacking sequence of [0/90/90/0], which was 0.4 mm in thickness, as shown in Fig. 6. The CNT fiber sensor for impact measurement was embedded between the first and second layers and the CNT fiber sensor for strain measurement was embedded between the third and fourth layers. Enamel insulated copper wires were embedded between the second and third layers and were connected with the ends of the CNT fiber sensors through the GFRP prepregs using silver paste. Therefore, at the center of the 1700 mm × 300 mm GFRP skin, a 300 mm long CNT fiber sensor was located perpendicular to the chord line direction for strain measurement, and a 200 mm long CNT fiber sensor was located parallel to the chord line direction for impact measurement. A 120 Ω strain gauge was also attached at the center of the GFRP skin at the bottom surface in the same direction as the CNT fiber sensor for strain measurement. The sensor adapter of the CNT fiber sensor, which was connected with the enamel wires, was located at the wing root, which was connected with the SHM sensor node located inside the fuselage.

The resistance of the CNT fiber sensor was extremely sensitive to temperature change. Although the surrounding GFRP skin did block some of the environmental effects, it was not able to act as a temperature insulator. After the 1700 mm × 300 mm GFRP skin was attached to the main wing structure, a precise thermocouple was attached to the GFRP skin beside the CNT fiber sensor location and an external small sized data logger (TR-75wb) with a resolution of 0.1℃ and an accuracy of 0.3℃ was used to measure the temperature difference. Since the size of the whole main wing was not able to be put inside a temperature chamber, it was exposed to two different lower temperature environments which resulted in temperature decreases of 3.3℃ and 1.5℃. For the full length of the experiment, the temperature was measured using the thermocouple and data logger with a 1 Hz sampling frequency and the strain measurement of the CNT sensor fiber using the wireless SHM sensor node was measured

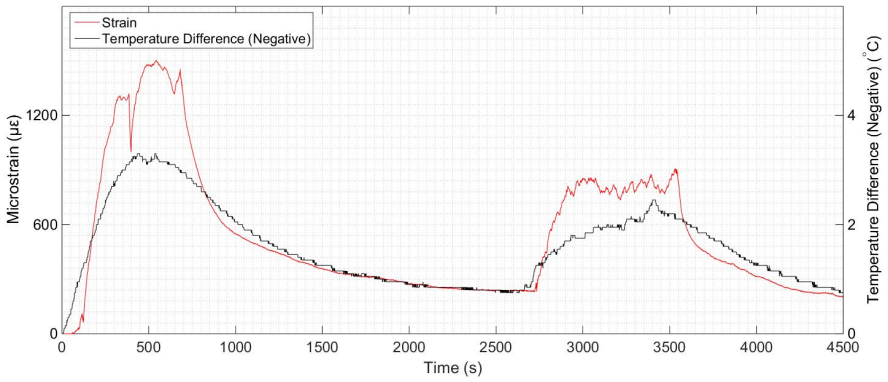

Fig. 7 Strain measurement of the CNT fiber sensor embedded inside the GFRP skin during temperature change

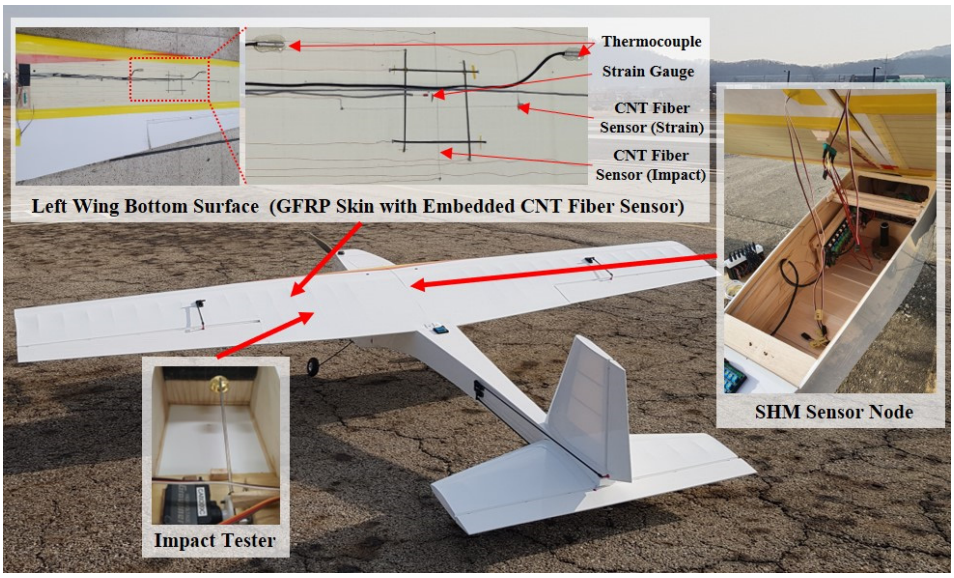

Fig. 8 Aircraft with SHM sensor node, GFRP skin and impact tester

with a 100 Hz sampling frequency as shown in Fig. 7. A temperature decrease of 3.3℃ induced a 1500 με strain increase and a temperature decrease of 1.5℃ induced a 900 με strain increase from the original state. Therefore, for every 0.1℃ decrease in temperature, an average increase of 50 με in strain was observed.

3.2 CNT fiber sensor embedded aircraft specification

The CNT fiber sensor embedded aircraft had a wingspan of 3.5 m, and the GFRP skin was attached at the bottom surface of the main left wing as shown in Fig. 8. Carbon fiber reinforced plastic (CFRP) pipe with a diameter of 30 mm was used for the spar of the aircraft for maximum deflection in order to measure strain with high sensitivity. A 2800 W brushless motor was used for the main thrust and a high-performance global navigation satellite system aided inertial navigation system (GNSS/INS) device (VN-200) was used to measure altitude, speed, and angle velocity of the aircraft during flight. The flight data was transferred from the aircraft to the ground station by MM2-T radio modem using 900 MHz frequency band. A remotely controlled impact tester was embedded inside the main wing, 400 mm from the impact measuring CNT fiber sensor. The impact tester consisted of a servo motor with a rotation plate and brass weight attached to a steel rod. When the servo motor was initiated wirelessly during flight test, the brass weight was elevated first and then dropped in order to simulate an impact.

4. In-flight measurements

During the flight test of the aircraft, both strain and impact were measured simultaneously. For strain measurement, both the CNT fiber sensor and the strain gauge took measurements at a sampling frequency of 100 Hz. Even though the strain measurement was measured for the full length of the flight, the strain measurement during takeoff and landing was indistinguishable from the strain difference induced from the temperature difference. Although the aircraft flew at a low altitude, the temperature difference during the flight was measured to be 0.5℃, which would increase the strain by 250 με according to the above temperature change experiment. Therefore, only the dynamic maneuvers were able to be measured for strain measurement. Fig. 9(a) shows the comparison between strain measurements from the CNT fiber sensor and strain gauge with pitch angular velocity. During this flight interval, the aircraft performed rapid fluctuation in altitude to maximize the wing deformation to simulate harsh maneuvers of the aircraft. The strain measurements from both the CNT fiber sensor and the strain gauge matched the pitch angular velocity. The average strain measurements of the wing deformation from the CNT fiber sensor and the strain gauge were 40 με and 70 με. Compared to the amplitude of the strain gauge strain measurement, the amplitude of the CNT fiber sensor strain measurement was smaller; however, it was still possible to interpret the wing deformation of the aircraft during harsh maneuvers. The cause for the difference in strain measurement can be mainly from the difference in gauge length of the two sensors. The gauge length of the CNT fiber sensor for strain measurement was 300 mm, where the gauge length of the strain gauge was 10 mm and was located at the center of the CNT fiber sensor. The CNT fiber sensor strain measurement was the average of the whole 300 mm gauge length which resulted smaller strain measurement than the strain gauge strain measurement. Therefore, decreasing the gauge length of the CNT fiber sensor may increase the accuracy of the strain measurement at a specific location but will decrease the measuring length and the mechanical properties of the composite structures. For impact measurement, the CNT fiber sensor was measured at 100 kHz. There was no incoming data until the impact tester was initialized since there was no sudden peak larger than the predefined threshold. During the flight, the impact tester was initialized

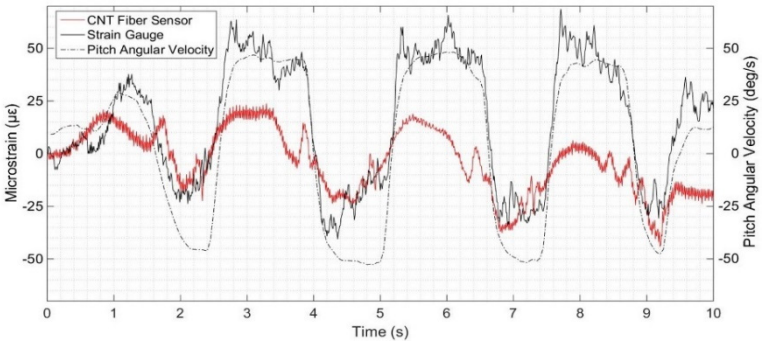

(a) Strain measurement of CNT fiber sensor and strain gauge

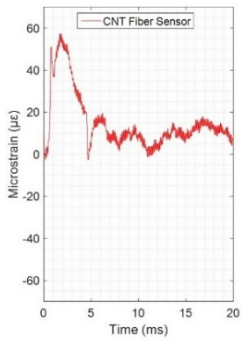

(b) Impact measurement of CNT fiber sensor

Fig. 9 SHM sensor node in-flight measurements

and 2000 data points after the peak were acquired wirelessly. Fig. 9(b) shows the measured impact. The highest peak from the impact was measured to be 55 με, and the attenuation of the impact was also measured. Since the length of the impact measurement for the 2000 data points was 20 ms, only the early phase of the impact was measured.

5. Conclusions

In this study, a compact and lightweight wireless SHM sensor node and a CNT based fiber sensor embeddable in composites were developed to monitor the structural integrity of a UAV during a flight in real time. The wireless SHM sensor node consisted of an analog sensing circuit capable of measuring an embedded CNT fiber sensor with high resistance. Additionally, a double buffering method and DMA transfer method with a long-range wireless protocol inside the MCU were used to transfer the continuous SHM data to the ground station from a distance of up to a few kilometers. The proposed CNT fiber sensors exhibited high mechanical properties and were only 80 μm in diameter, which enhanced the structural properties without creating delamination when embedded inside the composite structure. During the in-flight measurement, the wireless SHM sensor node exhibited a continuous 100 Hz sampling frequency for strain measurement and a self-triggering 100 kHz sampling frequency for impact measurement. Strain measurement from the CNT fiber sensor was compared with the strain gauge measurement and pitch angular velocity measurement for validation. In addition, an impact signal excited by the on-board impact tester was acquired by the CNT fiber sensor during the flight. The in-flight measurements from the embedded CNT fiber sensors and wireless SHM sensor node indicated the possibility of consistent SHM throughout the flight with minimum additional payload for small sized UAVs.

Acknowledgments

This work was supported by the Technology Innovation Program (10074278) funded by the Ministry of Trade, Industry & Energy (MI, Korea) and by the National Research Foundation of Korea (NRF) Grant funded by the Ministry of Science and ICT (NRF-2017R1A5A1015311).

References

Alvarez-Montoya, J., Carvajal-Castrillón, A. and Sierra-Pérez, J. (2019), "In-flight and wireless damage detection in a UAV composite wing using fiber optic sensors and strain field pattern recognition", *Mech. Syst. Signal Process.*, **136**, 106526. https://doi.org/10.1016/j.ymssp.2019.106526

Botelho, E.C., Silva, R.A., Pardini, L.C. and Rezende, M.C. (2006), "A review on the development and properties of continuous fiber/epoxy/aluminum hybrid composites for aircraft structures", *Mater. Res.*, **9**(3), 247-256. http://dx.doi.org/10.1590/S1516-14392006000300002

Hassan, M.H., Othman, A.R. and Kamaruddin, S (2017), "A review on the manufacturing defects of complex-shaped laminate in aircraft composite structures", *Int. J. Adv. Manuf. Technol.*, **91**, 4081-4094. https://doi.org/10.1007/s00170-017-0096-5

Herszberg, I., Bannister, M.K., Li, H.C.H., Thomson, R.S. and White, C. (2007), "Structural health monitoring for advanced composite structures", *Proceedings of the 16th International Conference on Composite Materials*, Kyoto, Japan, July.

Kim, K., Park, Y., Kim, Y.Y., Shrestha, P. and Kim, C.G. (2015), "Aircraft health and monitoring system for in-flight strain measurement of a wing structure", *Smart Mater. Struct.*, **24**(10), 105003. http://dx.doi.org/10.1088/0964-1726/24/10/105003

Kressel, I., Hangelman, A., Botsev, Y., Balter, J., Guedj, P., Gorbatov, N., Tur, M., Pillai, A., Prasad, M.H., Gupta, N., Joseph, A.M. and Sundaram, R. (2012), "Evaluation of flight data from an airworthy structural health monitoring system integrally embedded in an unmanned air vehicle", *Proceedings of the 6th European Workshop on Structural Health Monitoring*, Dresden, Germany, July.

Kwon, H., Park, Y., Kim, J. and Kim, C.G. (2019), "Embedded fiber Bragg grating sensor-based wing load monitoring system for composite aircraft", *Struct. Health Monitor.*, **18**(4), 1337-1351. https://doi.org/10.1177/1475921719843772

Molent, L. and Aktepe, B. (2000), "Review of fatigue monitoring of agile military aircraft", *Fatig. Fract. Eng. Mater. Struct.*, **23**(9), 767-785. https://doi.org/10.1046/j.1460-2695.2000.00330.x

On, S.Y., Park, S. and Kim, S.S. (2019), "Preparation and characterization of hybrid structured MWCNT/UHMWPE fiber sensors for strain sensing and load bearing of composite structures", *Adv. Mater. Technol.*, **4**(12), 1900807. https://doi.org/10.1002/admt.201900807

Staszewki, W.J., Mahzan, S. and Traynor, R. (2009), "Health

monitoring of aerospace structures-active and passive approach", *Compos. Sci. Technol.*, **69**(11-12), 1678-1685. https://doi.org/10.1016/j.compscitech.2008.09.034

Takeda, S., Minakuchi, S., Okabe, Y. and Takeda, N. (2005), "Delamination monitoring of laminated composites subjected to low-velocity impact using small-diameter FBG sensors", *Compos. Part A: Appl. Sci. Manuf.*, **36**(7), 903-908. https://doi.org/10.1016/j.compositesa.2004.12.005

Tang, A.N., Zhou, Z.T. and Cao, J.T. (2010), "A technique of landing gear loads calibration with strain gages", *Proceedings of 27th International Congress of the Aeronautical Sciences*, Nice, France, September.

Zhou, D., Ha, D.S. and Inman, D.J. (2010), "Ultra low-power active wireless sensor for structural health monitoring", *Smart Struct. Syst., Int. J.*, **6**(5), 675-687. https://doi.org/10.12989/sss.2010.6.5_6.675

Zhu, H., Wang, X., Liang, J., Lv, H., Tong, H., Ma, L., Hu, Y., Zhu, G., Zhang, T., Tie, Z., Liu, Z., Li, Q., Chen, L., Liu, J. and Jin, Z. (2017), "Versatile electronic skins for motion detection of joints enabled by aligned few-walled carbon nanotubes in flexible polymer composites", *Adv. Funct. Mater.*, **27**(21), 1606604. https://doi.org/10.1002/adfm.201606604

HJ